

On the effects of microphysical grain properties on the yields of carbonaceous dust from type II SNe

David W. Fallest^{1*}, Takaya Nozawa², Ken'ichi Nomoto², Hideyuki Umeda³, Keiichi Maeda², Takashi Kozasa⁴ and Davide Lazzati¹

¹ *Department of Physics, NC State University, 2401 Stinson Dr., Raleigh, NC 27695-8202*

² *Institute for the Physics and Mathematics of the Universe, University of Tokyo, Kashiwa 277-8583, Japan*

³ *Department of Astronomy, School of Science, University of Tokyo, Tokyo 113-0033, Japan*

⁴ *Department of CosmoSciences, Graduate School of Science, Hokkaido University, Sapporo 060-0810, Japan*

5 November 2018

ABSTRACT

We study the role of the unknown microphysical properties of carbonaceous dust particles in determining the amount and size distribution of carbonaceous dust condensed in type II supernova explosions. We parametrize the microphysical properties in terms of the shape factor of the grain and the sticking coefficient of gas-phase carbon atoms onto the grain surfaces. We find that the amount of dust formed is fairly independent of these properties, within the parameter range considered, though limited by the available amount of carbon atoms not locked in CO molecules. However, we find that the condensation times and size distributions of dust grains depend sensitively on the microphysical parameters, with the mass distributions being weighted toward larger effective radii for conditions considering grains with higher sticking coefficients and/or more aspherical shapes. We discuss that this leads to important consequences on the predicted extinction law of SN dust and on the survival rate of the formed grains as they pass through the reverse shock of the SN. We conclude that a more detailed understanding of the dust formation process and of the microphysical properties of each dust species needs to be achieved before robust prediction on the SN dust yields can be performed.

Key words: dust, extinction — supernovae: general

1 INTRODUCTION

Interstellar dust, once considered to be little more than a nuisance to astronomical observations, is one of the most interesting areas of astrophysical research today (Li & Greenberg 2003). One aspect of particular interest is the origin of dust at high redshift ($z > 5$). Possible sources of interstellar dust that have been considered include outflows from asymptotic giant branch (AGB) stars (Morgan & Edmunds 2003; Zhukovska, Gail, & Tieloff 2008; Valiante et al. 2009), Wolf-Rayet systems (Cherchneff 2010), quasars (Elvis, Marengo, & Karovska 2002), and supernova explosions (Kozasa, Hasegawa, & Nomoto 1989, 1991; Todini & Ferrara 2001; Nozawa et al. 2003; Bianchi & Schneider 2007; Kozasa et al. 2009; Cherchneff 2010). How much dust can be attributed to each of these possible sources at such high redshift remains unclear. Supernovae (SNe) are considered by some to be likely contributors of much of the dust in the early Universe

because their progenitors are quite massive and consequently have short lifetimes (Bromm, Coppi, & Larson 2002; Morgan & Edmunds 2003; Maiolino et al. 2004; Dwek, Galliano, & Jones 2007). However, such early SNe have not been observed, making determinations of their dust contributions difficult. Instead we need to consider dust yield predictions of more recent SNe, which have been observed, and then extrapolate the dust yields to earlier SNe. The theoretical predictions of dust yields for recent supernovae (Kozasa, Hasegawa, & Nomoto 1991; Todini & Ferrara 2001; Nozawa et al. 2008), however, are too large compared to observations, with discrepancies that can be as high as 3 to 4 orders of magnitude in some cases (Hoyle & Wickramasinghe 1970; Lucy et al. 1989; Wooden et al. 1993; Elmhamdi et al. 2003; Meikle et al. 2007; Kotak et al. 2009). Observations of young supernova remnants (SNR), however, have confirmed dust masses one to two orders of magnitude greater than SNe. Some of these SNR have observed dust masses of 0.02–0.054 M_{\odot} by *Spitzer* (Rho et al. 2008), 0.06 M_{\odot} by *AKARI* (Sibthorpe et al. 2010), and 0.075 M_{\odot} by *Herschel* (Barlow et al. 2010), in

* E-mail: dwfalles@unity.ncsu.edu

Cassiopeia A, and $0.04\text{--}0.1\text{ M}_{\odot}$ by *Spitzer* in the pulsar wind nebula G54.1+0.3 (Temim et al. 2010). Additionally, Nozawa et al. (2010) have demonstrated that the observed spectral energy distribution of Cassiopeia A can be well reproduced by the calculations of dust formation in Type IIb SNR and the mass in the SNR is 0.07 M_{\odot} .

Reconciling the dust yield prediction for local SNe can be done via one of two channels: improving our understanding of the dust formation process, leading to a substantially decreased prediction, or revising the observational constraints to account for a higher dust yield than so far implied. It is possible that some amount of dust has avoided observation. Dust particles absorb light and re-emit the energy at infrared wavelengths. However, cold dust at temperatures of a few tens of Kelvin could escape detection at mid-infrared wavelengths. Additionally, areas where the dust is optically thick could obscure some amount of dust, again allowing some dust to not be detected. Dust clumping may also affect the estimates of dust mass from absorption (Sugerman et al. 2006), since it is usually assumed that the surface filling factor of dust is close to unity, while substantial clumping could be present due to the intrinsic inhomogeneity of the ejecta and Rayleigh-Taylor instabilities in the expanding ejecta (Wooden 1997; Douvion, Lagage, & Cesarsky 1999).

On the theoretical side, all the estimates for dust production in SNe are based on the so-called classical theory of nucleation (e.g., Becker & Döring (1935)). It has been argued, however, that the use of classical nucleation theory in astrophysical environments is questionable (Donn & Nuth 1985; Lazzati 2008). In addition, almost all SN dust nucleation models thus far have considered the formation of spherical grains, and assumed any atoms/molecules that contact the grain will adhere to the grain; conditions that reflect maximally efficient nucleation. It is therefore not entirely surprising that the theoretical estimates of SN dust yields, based on upper limit of nucleation efficiency, are in excess of those from observations. It should be noted that Bianchi & Schneider (2007) have considered less than maximally efficient nucleation by assuming the probability of atoms/molecules adhering to the grain is less than unity, resulting in smaller dust yields.

Since dust formation is a highly non-linear phenomenon, understanding the effects of different nucleation rates on the final dust yields is difficult. To check the effects of different nucleation conditions we have performed a parametric study, in which we consider carbonaceous dust production in a SN explosion by varying the shape of the forming grains as well as the sticking coefficient, i.e., the probability that an incoming monomer will stick to the grain rather than bounce off and remain in the gas phase. Our study is phenomenological and aims at understanding which conclusions of previous nucleation studies are robust to changing the parameters, and which may need to be investigated more thoroughly. A self-consistent nucleation model in astrophysical conditions will be achieved by involving a kinetic approach (Donn & Nuth 1985; Lazzati 2008; Keith & Lazzati 2011) and detailed chemistry of precursor molecules (Cherchneff & Dwek 2009, 2010). Such a detailed approach, however, is still under development and is not yet applicable to large scale simulations like the one that we use here, and that have been used in previous investigations of e.g., Todini & Ferrara (2001); Nozawa et al. (2003, 2010).

This paper is organized as follows: in Sect. 2 we detail the nucleation theory that we adopted; in Sect. 3 we describe the numerical code used for the computations; and in Sect. 4 we describe our results. In Sect. 5 we finally discuss the implication and limitations of our results and lay out future perspectives for SN dust studies.

2 NUCLEATION

Nucleation is the first step of a first-order phase transition. In the case we consider here, the phase transition is from a gas of carbon atoms to solid clusters of amorphous carbon dust. There is a phase equilibrium pressure where both the gas and solid phases are stable within a given volume. The phase equilibrium pressure depends on the temperature of the materials in the gas phase within the volume. Nucleation of clusters of atoms/molecules of the new phase is favoured when the gas phase is supersaturated (i.e., the pressure of the gas is higher than the phase equilibrium pressure). The higher the supersaturation (i.e., the ratio of the pressure to the phase equilibrium pressure), the smaller the size of the stable clusters that are able to form. The size of the smallest stable cluster able to form at a given temperature and density is called the critical cluster size. Clusters that are smaller than the critical size will tend to evaporate, while larger clusters will tend to continue to grow. The goal of any nucleation theory is to calculate how many critical clusters form per unit volume per unit time.

The classical theory of nucleation considers nucleation as a thermodynamical process in quasi-equilibrium (Becker & Döring 1935; Feder et al. 1966; Kashchiev 2000). Besides the supersaturation level, the physical properties of the nucleating material affect the size of a critical cluster. The classical nucleation theory assumes that all clusters share the same properties, such as surface tension and shape, independent of their size. The theory also assumes that those properties are equal to those of a macroscopic sample. Moreover, the clusters are assumed to have a uniform equilibrium temperature that is equal to the temperature of the surrounding gas. These basic assumptions are problematic because macroscopic thermodynamic properties are not expected to be applicable to clusters of only a few atoms.

A different approach is provided by the kinetic theory of nucleation, which is applicable to very small cluster sizes. The kinetic theory relies on calculating the attachment and detachment frequencies of monomers to a cluster (Kashchiev 2000). Furthermore, in contrast to the classical nucleation theory, the kinetic theory follows the formation of clusters smaller than the critical cluster size. In the framework of the kinetic theory the critical cluster is the cluster whose attachment and detachment frequencies are equal, and thus it is stable. The downside of the kinetic theory is that attachment and detachment frequencies for all cluster sizes need to be calculated in order to determine the overall nucleation rate. The main aim of this paper is to reveal the dependence of dust formation processes on the microphysical properties of grains. In order to achieve this, we adopt the simpler classical nucleation theory, rather than using the kinetic theory that demands a more complicated treatment.

When the supersaturation level is $S > 1$, nucleation can

take place because the free energy of the new phase is lower than that of the old phase (Kashchiev 2000). The change in the free energy is due to the work necessary to form the critical size clusters. Energy is released in the formation of the volume of the cluster, but energy is required in order to form the surface of the cluster (Kashchiev 2000). The nucleation rate (Eq. (1)) is given basically by two factors: the number density of critical clusters and a kinetic factor that describes the rate at which clusters become large enough to be stable (i.e., critical size or larger).

The general equation of stationary nucleation is given by (Kashchiev (2000), their equation 13.39):

$$J_S = A \exp(-W^*/kT), \quad (1)$$

where A is the kinetic factor, W^* is the work needed to form the critical size cluster from the gaseous state, k is the Boltzmann constant, and T is the gas temperature. The kinetic factor, A , is given by $A = A' \exp(\Delta\mu/kT)$, and A' is:

$$A' = \gamma^* \left(\frac{c^3 \sigma}{18\pi^2 m_0} \right)^{\frac{1}{2}} \left(\frac{p_e v_0}{kT} \right) C_0,$$

where γ^* is the size dependent sticking coefficient, c is the shape factor of the cluster, σ is the surface tension, m_0 and v_0 are, respectively, the mass and volume of the monomer of nucleating material, p_e is the phase-equilibrium pressure, and C_0 is the concentration of sites where nucleation can occur (equations 13.41 and 13.44, respectively in Kashchiev (2000)). The concentration of gaseous monomers, C_1 is related to the concentration of nucleation sites by $C_1 = C_0 \exp(-W_1/kT)$, where W_1 is the work needed to form a cluster consisting of one monomer (equation 7.5 in Kashchiev (2000)). We consider the monomer in the gaseous state to be indistinguishable from the monomer in the condensed state, so that $W_1 = 0$ and $C_1 = C_0$. Using the supersaturation ratio, $S = C_1/C_{1,e} = p/p_e$ and $\Delta\mu = kT \ln S$, where $C_{1,e} = p_e/kT$ is the gaseous monomer concentration at the phase-equilibrium pressure and p is the partial pressure of gaseous monomers, we obtain

$$A = \gamma^* \left(\frac{c^3 v_0^2 \sigma}{18\pi^2 m_0} \right)^{\frac{1}{2}} C_1^2.$$

While the sticking coefficient may depend on the size of the cluster, we consider it to be constant, so that $\gamma^* = \gamma = \text{constant}$. Finally, using the work to form a critical sized cluster $W^* = 4c^3 v_0^2 \sigma^3 / 27 \Delta\mu^2$ (Kashchiev (2000), equation 4.8), we find our stationary nucleation rate equation to be:

$$J_s = \gamma \left(\frac{c^3 v_0^2 \sigma}{18\pi^2 m_0} \right)^{\frac{1}{2}} C_1^2 \exp \left(\frac{-4c^3 v_0^2 \sigma^3}{27(kT)^3 (\ln S)^2} \right). \quad (2)$$

After nucleation the clusters grow through impingement of monomers upon the cluster. To find how much the clusters grow we begin by finding the volume of the newly nucleated cluster. The clusters nucleate with some critical number of monomers, n^* (equation 4.7 in Kashchiev (2000)):

$$n^* = \frac{8c^3 v_0^2 \sigma^3}{27 \Delta\mu^3}. \quad (3)$$

The volume of the critical cluster is then, $v^* = n^* v_0$. The change in the cluster's volume over time depends on the sticking coefficient γ , the surface area of the cluster Σ , the

concentration of monomers C_1 , the volume of the monomer v_0 , and the average relative speed of the monomers with respect to the cluster. In this paper we consider clusters that can nucleate with aspherical shapes through the use of the shape factor c . The shape factor is a dimensionless quantity that relates the surface area Σ of an object to its volume V by: $c = \Sigma/V^{2/3}$ (Kashchiev 2000). Thus we find the change in volume over time to be:

$$\frac{dV}{dt} = \gamma c V^{\frac{2}{3}} C_1 v_0 \left(\frac{kT}{2\pi m_0} \right)^{\frac{1}{2}}. \quad (4)$$

In the same manner as Nozawa et al. (2003) we compute the depletion of the available nucleation material through mass conservation:

$$1 - \frac{C_1(t)}{\tilde{C}_1(t)} = 1 - Y_1 = \int_{t_e}^t \frac{J(t')}{\tilde{C}_1(t')} \frac{V(t, t')}{v_0} dt', \quad (5)$$

where \tilde{C}_1 is the nominal concentration of monomers – the concentration expected should nucleation not occur, which in an expanding shell of volume V_{shell} can be found using

$$\tilde{C}_1(t = t_n) V_{shell}(t = t_n) = \tilde{C}_1(t = t_0) V_{shell}(t = t_0),$$

so that the total number of gas-phase atoms remains constant, and $V(t, t')$ is the volume of a cluster formed at time t' and measured at time t . Rather than computing the integral on the right-hand side, we instead calculate $C_1(t)$ as described in step (iii) in the next section. From Eqs. (2) and (4), we see that J_s and dV/dt are simply proportional to the sticking coefficient γ . Thus, we expect that reduced sticking coefficients will suppress both nucleation and grain growth. The dependence of J_s on the shape factor c is more complicated, since it appears in both the kinetic factor and the exponential term. The shape factor in the exponential term, however, will dominate the nucleation rate equation and we expect that increased shape factors will suppress nucleation. On the other hand, grain growth (dV/dt) is simply proportional to c , and thus an increase in the shape factor will increase the cluster growth rate.

3 SIMULATIONS

We concentrate on the formation of carbonaceous grains (clusters) from carbon atoms in the expanding material of a core-collapse supernova. Our simulations are based on the hydrodynamic results and elemental composition for the unmixed ejecta of a core-collapse supernova of a 20 M_\odot progenitor star with metallicity $Z = 0$ and an explosion energy of 10^{51} ergs by Umeda & Nomoto (2002) (see also Nomoto et al. (2006)).

Table 1 describes the data necessary for the calculation of carbon grain formation. To compute the supersaturation of the expanding gas, we find the phase equilibrium pressure by: $p_e = p_0 e^{-A/T+B}$, where p_0 is the standard pressure, T is the temperature, and the values of A and B , listed here in Table 1, are taken from Table 2 of Nozawa et al. (2003). As the material ejected by the core-collapse supernova expands it also cools. Figures 1 and 2 show the evolution of the density and temperature, respectively, of the expanding and cooling material for two of the enclosed mass subshells that we refer to in the rest of this work.

We study four different values of the unknown sticking

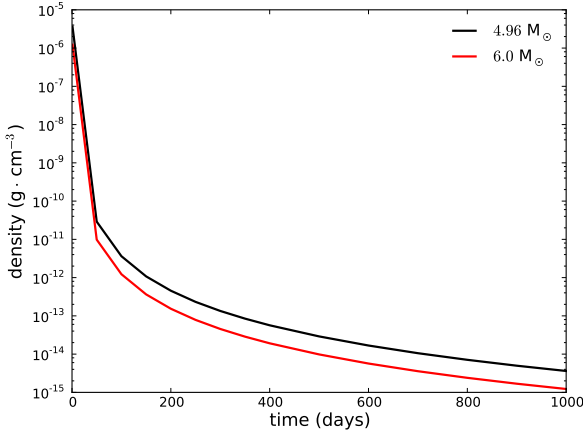


Figure 1. Density evolution for 4.96 (black) and 6.0 (red) M_{\odot} enclosed mass subshells up to 1000 days after the SN explosion.

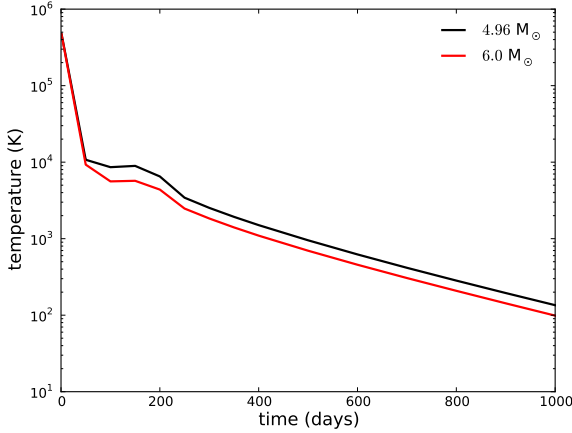


Figure 2. Temperature evolution for 4.96 (black) and 6.0 (red) M_{\odot} enclosed mass subshells up to 1000 days after the SN explosion.

coefficient, $\gamma = 1.0, 0.1, 0.01$, and 0.001 , neglecting any dependence of γ on the temperature of the gas and the size of the cluster. For each value of the sticking coefficient, we study six different values for the shape factor, $c = (36\pi)^{1/3}, 5.4, 6.0, 7.0, 9.0$, and 12.0 , corresponding to shapes ranging from a sphere to a flattened cylinder similar to a coin. We therefore performed 24 simulations in total. A sticking coefficient of $\gamma = 1.0$, and a shape factor for a sphere of $c = (36\pi)^{1/3}$ are the usual parameters used in previous nucleation works.

As in Nozawa et al. (2003), we assume that the stable formation of CO molecules occurs prior to grain nucleation and that carbon grains will form only where the initial num-

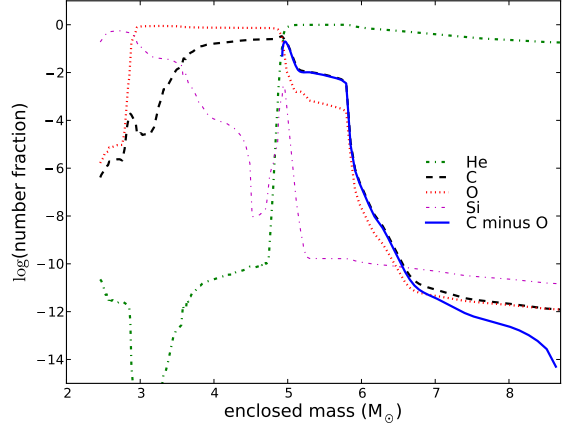


Figure 3. Number fraction of helium (green dash-dot), carbon (black dashed), oxygen (red dotted), and silicon (magenta dash-dot) atoms for enclosed masses from 2.45 to 8.7 M_{\odot} . The solid (blue) line is the carbon number fraction after the formation of CO molecules.

ber fraction of carbon is higher than that of oxygen. Under this assumption, the number fraction of free carbon atoms available for dust formation is obtained simply from the initial number fraction of carbon minus the number fraction oxygen. We divide the expanding gases into a series of enclosed mass shells beginning at $\sim 4.93 M_{\odot}$ and ending at $\sim 6.21 M_{\odot}$. In this range of enclosed masses the number fraction of carbon atoms, after the formation of CO, is highest; ranging between 2×10^{-1} and 8×10^{-9} . Figure 3 shows the number fraction of carbon and oxygen atoms in the expanding ejecta from the hydrodynamic results of Umeda & Nomoto (2002). The solid (blue) line indicates the number fraction of carbon left over after the formation of CO molecules. It should be noted for completeness that grain nucleation can occur at enclosed masses larger than we consider here, but is extremely inefficient due to low carbon number fractions, $\sim 10^{-14}$ and below.

For each mass subshell, our code starts by following the evolution of the density and temperature (see Figures 1 and 2, respectively, for examples) of the gas until the condition of supersaturation is satisfied. From that point on, at each time step the code performs three operations.

(i) First, the code computes the number of critical clusters that are formed given the saturation, temperature, and partial pressure of the carbon atoms (according to Eq. (2)).

(ii) Second, the code grows any pre-existing grain formed at earlier times according Eq. (4).

(iii) Finally, the code subtracts from the carbon in the gas phase the amount of carbon that has been locked in the solid phase by the processes in steps (i) and (ii). The concentration of gas-phase carbon is evolved according to:

$$C_1(t_n) = C_1(t_{n-1}) - \frac{\Delta V_{grains,n}}{v_0 V_{shell,n}} - \frac{C_1(t_{n-1})}{\tilde{C}_1(t_n)} (\tilde{C}_1(t_{n-1}) - \tilde{C}_1(t_n)),$$

where $\Delta V_{grains,n}$ is the total change in volume of grains from the previous time step to the current time step. Then, the

Table 1. Carbon properties

$A/10^4$ (K)	B	σ (erg·cm ⁻²)	v_0 (10 ⁻²⁴ cm ⁻³)	m_0 (10 ⁻²³ g)
8.64726	19.0422	1400	8.805	1.995

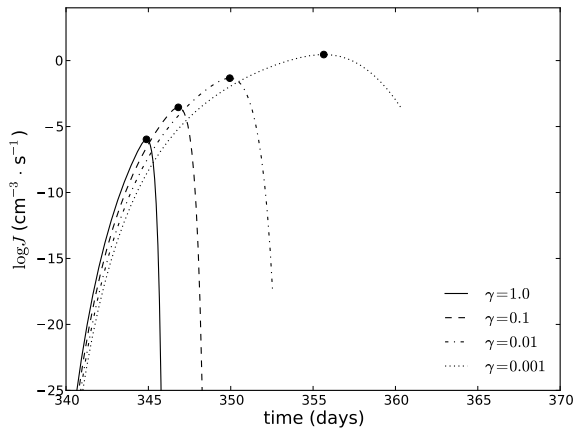


Figure 4. Nucleation rates for spherical grains ($c = (36\pi)^{1/3}$), for the four considered sticking coefficients of $\gamma = 1.0, 0.1, 0.01$, and 0.001 . Filled circles indicate the time and rate of maximum nucleation. Rates are calculated at an enclosed mass coordinate $4.96M_{\odot}$.

first term on the right-hand side is the concentration of gas-phase carbon from the previous time step, the second term is the change in the concentration of solid-phase carbon (it is a summation of all grain changes, including formation of new critical clusters and the growth of existing grains), and the final term accounts for the decrease in concentration of gas-phase carbon due to the expansion of the shell.

This process is repeated for each mass shell until the concentration of gas-phase carbon is reduced to 1 per cent of its original value. The dust distributions from all shells are then summed together to produce the final dust yield of each particular set (γ, c) .

4 RESULTS

4.1 Spherical Grains

After the supernova explosion, the hot gases expand and cool. The cooling allows the gases to reach supersaturation conditions. Once the supersaturation level becomes greater than unity, nucleation can occur. The supersaturation level continues to rise and the nucleation rate increases over time until depletion of available material becomes significant and the supersaturation level begins to drop, after which the nucleation rate falls off quickly. Eventually the gas is no longer supersaturated and nucleation ceases. However, grain growth is still possible.

Figure 4 shows the nucleation rate for spherically shaped grains at enclosed mass coordinate $4.96 M_{\odot}$ for the four sticking coefficients. We chose this particular enclosed mass shell because it contains the highest abundance of carbon atoms, after CO formation, of all our mass shells. The solid curve corresponds to $c = (36\pi)^{1/3}$ and $\gamma = 1.0$, the parameters generally used for nucleation studies. The dashed, dash-dot, and dotted curves correspond to $\gamma = 0.1, 0.01$, and 0.001 , respectively. To be consistent with the works of Kozasa & Hasegawa (1987); Kozasa, Hasegawa, & Nomoto (1989, 1991); Nozawa et al. (2003), we consider the time at

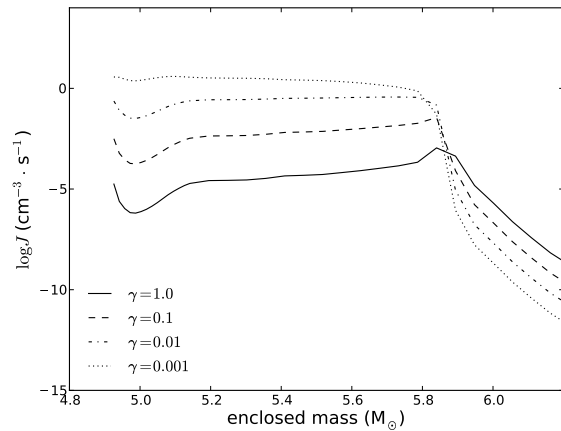


Figure 5. Maximum nucleation rates for spherical carbon grains at enclosed masses $< 6.2 M_{\odot}$ for four sticking coefficients.

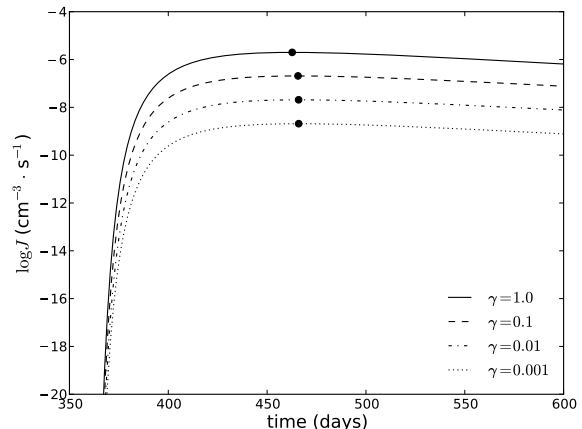


Figure 6. Nucleation rates for spherical carbon grains at an enclosed coordinate of $6.00 M_{\odot}$ for four sticking coefficients. Condensation times are indicated by filled circles.

which the nucleation rate is at its maximum to be the condensation time of the grains. We show these condensation times as filled circles at the maxima of the nucleation rates in the figure.

At early times, the reduced sticking coefficient makes the formation of critically sized grains more difficult and results in a suppressed nucleation rate. In the absence of strong nucleation, carbon atoms are not depleted from the gas and the saturation continues to increase. The reduced sticking coefficient thus causes the time at which nucleation is at its maximum to be delayed, and the nucleation to take place at higher saturation levels. As a consequence, a larger number of critical clusters can form with much smaller size (Eq. 3).

Figure 5 shows the maximum nucleation rates for spherical grains as a function of enclosed mass for our four sticking coefficients. For enclosed masses up to $M_r \sim 5.87 M_{\odot}$, the nucleation rate maxima for reduced sticking coefficients exhibit similar behaviour as in Figure 4. At greater enclosed masses, however, the behaviour is inverted and a reduced

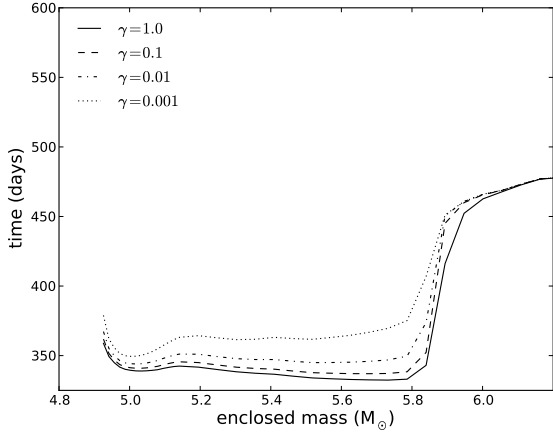


Figure 7. Condensation times of spherical carbon grain as a function of enclosed mass for four sticking coefficients.

sticking coefficient results in depressed maximum nucleation rates. This difference in behaviour is due to the reduction in the number fraction of carbon available, from $\sim 10^{-2.5}$ to $\sim 10^{-5}$ (see Figure 3), which corresponds to a reduction in the concentration of carbon monomers. Since the nucleation rate (Eq. (2)) is proportional to the concentration of monomers squared, the drop in the carbon concentration consequently drops the nucleation rate. Thus, the nucleation rates do not peak as strongly (Figure 6), drawing out nucleation to later times for all sticking coefficients, so that a catastrophic reduction in the available material does not occur. Thus, the nucleation rates for reduced sticking coefficients remain depressed throughout the simulation time for higher enclosed mass shells.

Figure 7 shows the condensation times corresponding to the maximum nucleation rates shown in Figure 5. The condensation times of the solid curve ($c = (36\pi)^{1/3}$, $\gamma = 1.0$) are in good agreement with the condensation times for carbon grains reported in Nozawa et al. (2003). Here the lower sticking coefficients result in delayed condensation times up to $M_r \sim 5.87 M_\odot$, outside which the condensation time is only slightly delayed, or no longer delayed, when compared to the case of $\gamma = 1.0$. The more noticeably delayed condensation times, as well as the similarity of condensation times for all our sticking coefficients, at higher enclosed mass shells are also due to the drawn out nucleation process already discussed above.

Reducing the sticking coefficient makes both nucleation and grain growth more difficult. A reduced sticking coefficient results in a larger number of smaller grains, fewer larger grains, and a smaller maximum grain radius. In Figures 8 and 9, respectively, we show the size and mass distributions for spherical grains. For the case of $\gamma = 1.0$, the maximum grain size achieved is between 2 and 3 μm . When the sticking coefficient is reduced to 0.001, the maximum grain size is decreased to less than 0.01 μm .

Since the reduced sticking coefficient causes larger numbers of small grains to form, the small grains contain more relative mass than the larger grains, as can be seen in Figure 9. However, the total mass of the grains is relatively robust. The total masses of dust grains for the spherical

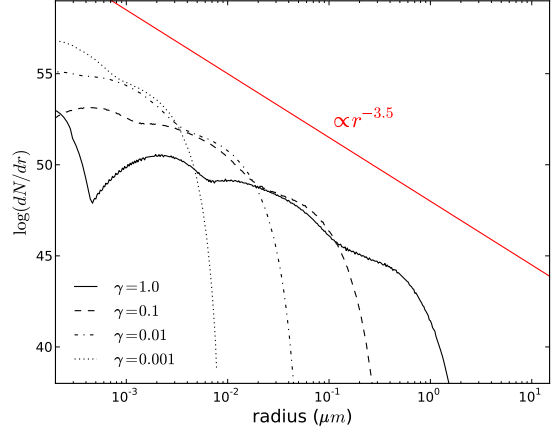


Figure 8. Size distribution of carbon grains for $\gamma = 1.0, 0.1, 0.01, 0.001$, with $c = (36\pi)^{1/3}$. For reference, the solid (red) line represents the power-law distribution with the form of $N_r \propto r^{-3.5}$, which has been suggested as that of interstellar grains (e.g., Mathis, Rumpl, & Nordsieck (1977)).

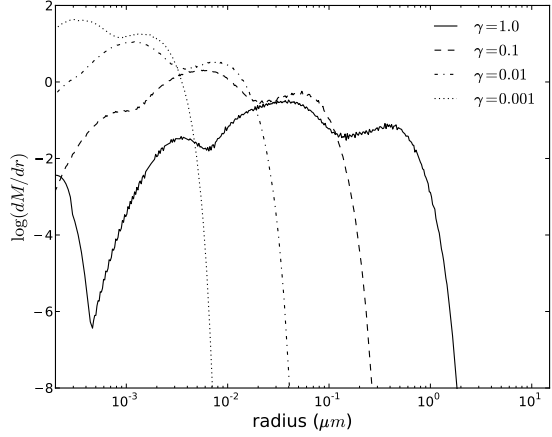


Figure 9. Mass distribution of carbon grains for $\gamma = 1.0, 0.1, 0.01, 0.001$, with $c = (36\pi)^{1/3}$.

case are shown in Table 2, along with the aspherical cases which are discussed in the next section. Even though the onset of nucleation is delayed due to the reduced sticking coefficient at enclosed masses less than $5.87 M_\odot$, where the majority of available carbon is contained, the subsequent grain growth consumes almost all of the carbon atoms for $\gamma > 0.001$. Thus, the total mass of carbon dust is principally determined by the mass of pre-existing carbon atoms.

4.2 Non-spherical Grains

We also calculated nucleation rates for aspherical grains. We choose a range of shape factors from $c = 5.4$ to $c = 12.0$. While $c = 6.0$ is the shape factor of a cube, each shape factor can correspond to a number of different grain shapes. The shape factor can be thought of as a deviation from the spherical case, the bigger the shape factor, the larger the

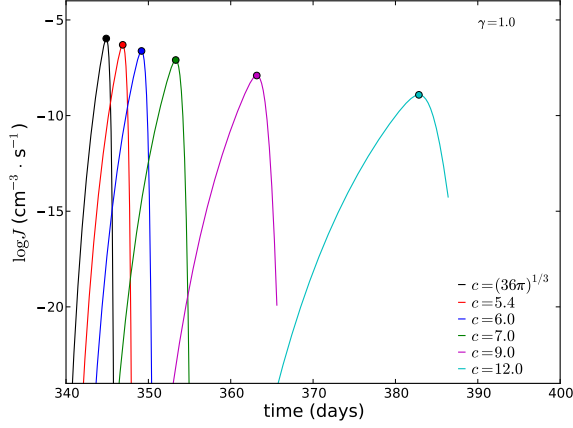


Figure 10. Nucleation rates as a function of time for six shape factors with $\gamma = 1.0$. Filled circles indicate maximum nucleation rate. Rates shown are for nucleation within a shell of enclosed mass of ~ 4.96 to $\sim 4.97 M_{\odot}$.

deviation from a sphere and the larger the surface for a given volume.

In Figure 10 we show the nucleation rates for the same enclosed mass shell as shown in Figure 4, for increasing shape factors with $\gamma = 1.0$. Since the shape factor appears in the exponential term of the nucleation rate equation as $J_s \propto \exp(-c^3)$ (Eq. (2)), the higher shape factors reduce the nucleation rate. Therefore, the higher supersaturation levels at later times need to be attained so that the nucleation rate becomes high enough for significant depletion of the gas due to the growth of newly formed grains. However, the maximum nucleation rates for increasing shape factors are decreased. This is due to the fact that with a larger surface to volume ratio aspherical grains tend to grow faster, producing a sizeable depletion of the gas-phase carbon even for moderate nucleation rates. For all mass coordinates, increasing the shape factor leads to lower nucleation rates and delayed condensation times (Figures 11a and 12a, respectively).

In Figure 11b–d we show the nucleation rate maxima for all shape factors for each of the other three sticking coefficients. For any sticking coefficient, the shape factor has the same effect of suppressing the nucleation rate. All condensation times, shown in Figure 12b–d, increase with the increased shape factor. Furthermore, for reduced sticking coefficients, greater shape factors lead to greater delays in the condensation time.

The shape factor $c = (36\pi)^{1/3}$ is the only shape factor that has just one associated shape, the sphere. The other shape factors we consider do not necessarily have a unique grain shape. To find a size distribution that is easily comparable to the spherical case, we define a *volume equivalent radius* for the aspherical grains as:

$$r_{\text{eff}} = \left(\frac{3V}{4\pi} \right)^{1/3}, \quad (6)$$

where V is the grain volume.

Figures 13a–d show the size distributions for all shape factors and sticking coefficients. As the shape factor is increased, the size and number of larger grains also increases.

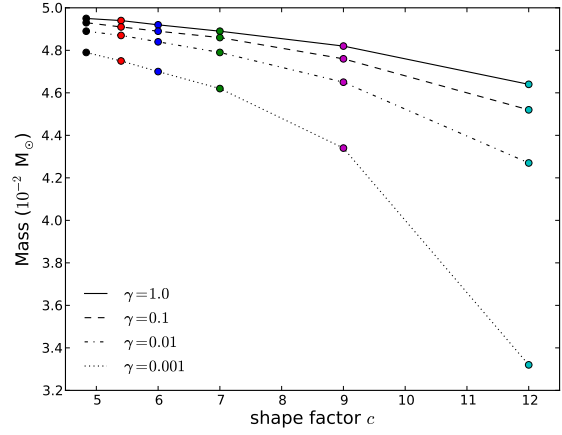


Figure 15. Total mass of carbon dust formed for all simulations.

Table 2. Total mass of carbon grains formed

Mass ($10^{-2} M_{\odot}$)				
c	$\gamma = 1.0$	$\gamma = 0.1$	$\gamma = 0.01$	$\gamma = 0.001$
$(36\pi)^{1/3}$	4.95	4.93	4.89	4.79
5.4	4.94	4.91	4.87	4.75
6.0	4.92	4.89	4.84	4.70
7.0	4.89	4.86	4.79	4.62
9.0	4.82	4.76	4.65	4.34
12.0	4.64	4.52	4.27	3.32

We find that the largest maximum grain radii are formed with $c = 12.0$ and $\gamma = 1.0$, and have a volume equivalent radius of almost $18 \mu\text{m}$. On the other hand, the smallest maximum grain radii ($\sim 0.008 \mu\text{m}$) are formed with $c = (36\pi)^{1/3}$ and $\gamma = 0.001$. As the sticking coefficient is reduced, the maximum grain radii for each shape factor are also reduced, and the number of smaller grains is increased. Even though there is a much larger number of small grains than large grains, the majority of the dust mass is contained within intermediate sized grains. In Figure 14a ($\gamma = 1.0$), most of the dust mass is contained in grains with volume equivalent radii between 0.01 and $0.5 \mu\text{m}$.

The masses of carbon grains formed (Figures 14a–d) are dominated by the relatively small numbers of larger sized grains as the shape factor is increased. However, as the sticking coefficient is reduced (Figures 14b–d), even the masses of the grains formed with the largest shape factor become dominated by the smaller sized grains. The total mass of carbon grains formed for increased shape factors is given in Table 2 and shown in Figure 15. Again, we notice that despite the difference in the size distribution due to different microphysical parameters, the total mass of dust that condenses is fairly robust (within a factor of 1.5) and constitutes almost the total amount of carbon that was left in the gas phase after the creation of CO molecules.

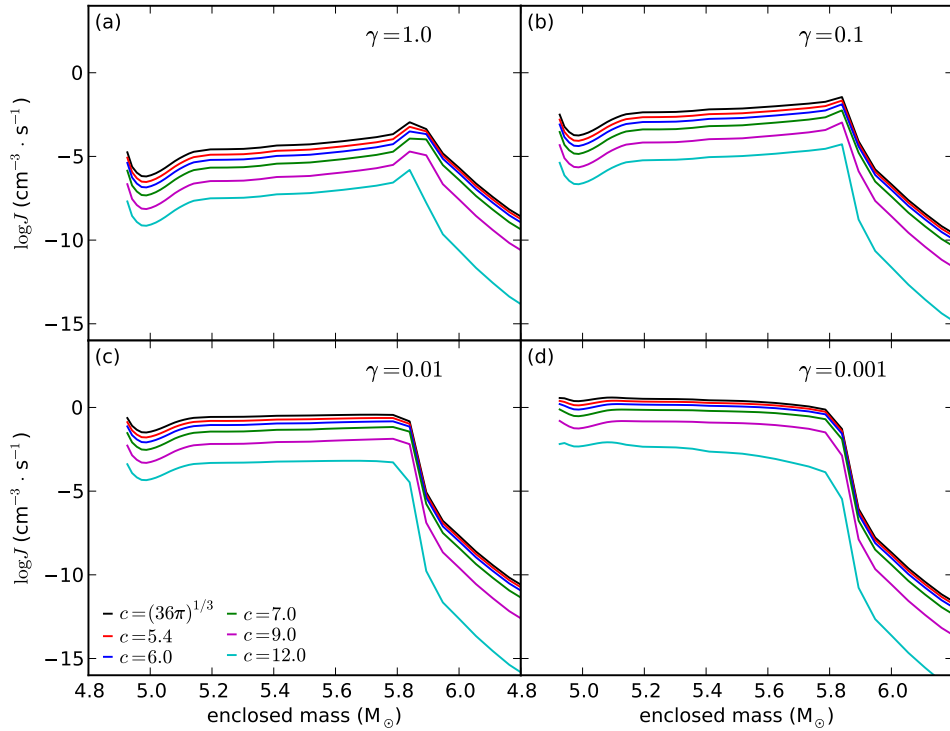


Figure 11. Maximum nucleation rates for all six shape factors and four sticking coefficients.

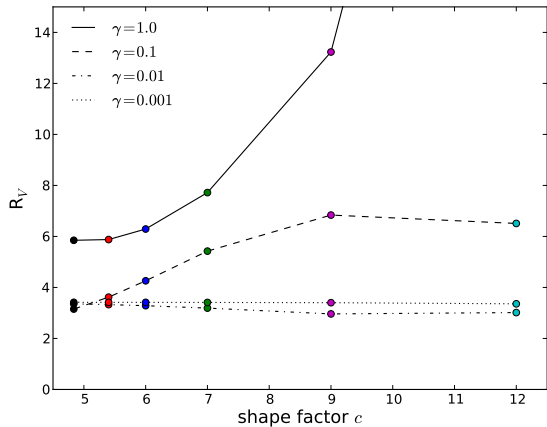


Figure 17. R_V values for 23 simulations. Not shown is $R_V = 41$ for $c = 12.0$ and $\gamma = 1.0$.

5 DISCUSSION

We have shown that varying the microphysical properties of dust grains has important effects on the condensation times, nucleation rates, and size distributions of carbon dust grains from type II supernova explosions. However, the total mass of dust is only modestly affected by the changes in the grain properties. An inadequate choice of the shape or sticking coefficient is not therefore a viable explanation for

the discrepancy between the mass of dust grains predicted in SN explosions and the observed dust mass in local type II SNe (see Section 1 for a more thorough discussion and references).

We find that a larger saturation is necessary to achieve efficient nucleation with either a small sticking coefficient ($\gamma < 1$) or for aspherical grains ($c > (36\pi)^{1/3}$). For that reason, all our simulations show that the condensation time grows when sticking coefficients less than unity or grain shapes that are different from spherical are adopted. However, differences can be found in the nucleation rates and final size distribution of the grains. Simulations with a low value of the sticking coefficient show a delayed nucleation but very high nucleation rates, thereby producing large quantities of small grains. This is due to the fact that low sticking coefficients inhibit both nucleation and grain growth and, therefore, all the carbon remains in the gas phase until a high saturation level is reached. At that point, many small grains are nucleated and the atomic carbon is quickly depleted. Bianchi & Schneider (2007) found similar effects when calculating dust nucleation with a sticking coefficient of $\gamma = 0.1$. Asphericity of the grains, on the other hand, inhibits nucleation but enhances grain growth. As a consequence, even if fewer grains are nucleated, they grow fast and the result is a grain size distribution characterized by less numerous, larger grains.

We find that the total mass of carbonaceous dust formed remains relatively stable even with sticking coefficients as low as 0.001. For the spherical case only, we ex-

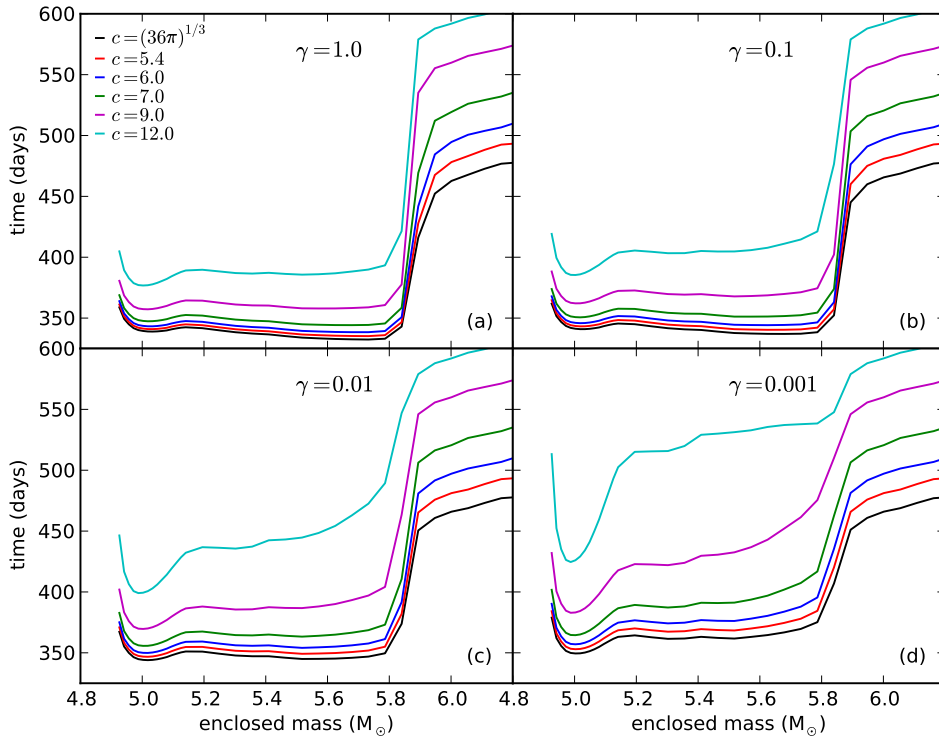


Figure 12. Condensation times for six shape factors and four sticking coefficients.

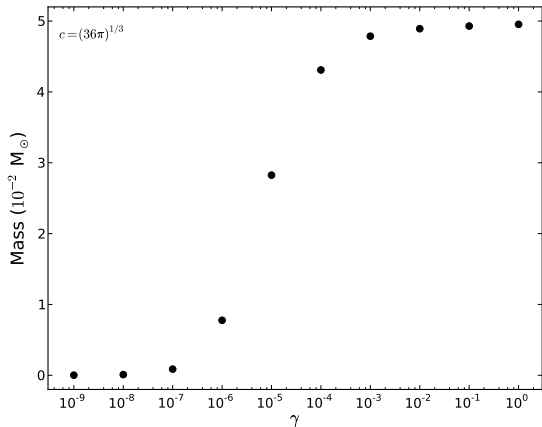


Figure 18. Total mass of dust formed for spherical carbonaceous grains with sticking coefficients down to $\gamma = 10^{-9}$.

explored the possibility of even smaller sticking coefficients, down to $\gamma = 10^{-9}$. We find that the mass of carbon dust formed becomes significantly reduced for sticking coefficients of $\gamma = 10^{-7}$ and below (see Figure 18). With sufficiently low values of sticking coefficient (below 10^{-8}) there is virtually no dust formation, but the required sticking coefficients seem unphysically low.

In terms of the observable properties of the SN-condensed dust, we find that the quantity that is most af-

fected is the extinction curve (see Figure 16). Not surprisingly, simulations with small sticking coefficient (which, as explained above, produce large amounts of small grains), result in a very steep extinction curve at far-UV wavelengths, with R_V values between 3 and 3.5, shown in Figure 17. We make special note that the R_V values for $\gamma = 1.0$ are relatively high, even though the size distribution of the grains is consistent with that of interstellar grains (see Figure 8), because we account for only carbon grains and that including other grains, such as silicates, could decrease the R_V values. On the other hand, simulations with very aspherical grains and relatively high sticking coefficients produce larger grains and, consequently, grey extinction curves. Without the knowledge of the values of the sticking coefficient and of the shape factor it is therefore impossible to predict the extinction curve of SN-condensed dust. This is a particularly worrying conclusion since the extinction curve is relatively easy to measure, even at high redshift, and could be used as an observational constraint for the origin of dust in the various environments. For example, Maiolino et al. (2004) compared the extinction curve measured in a quasar at $z = 6.2$ to the extinction curve calculated using the dust model by Todini & Ferrara (2001). They find that the data and the theoretical prediction are in good agreement and conclude that the dust observed in SDSSJ104845.05+463718.3 is indeed condensed in SN explosions (see also Stratta et al. (2007)). In light of our results, such conclusions need confirmation once a complete theory of SN dust nucleation is obtained.

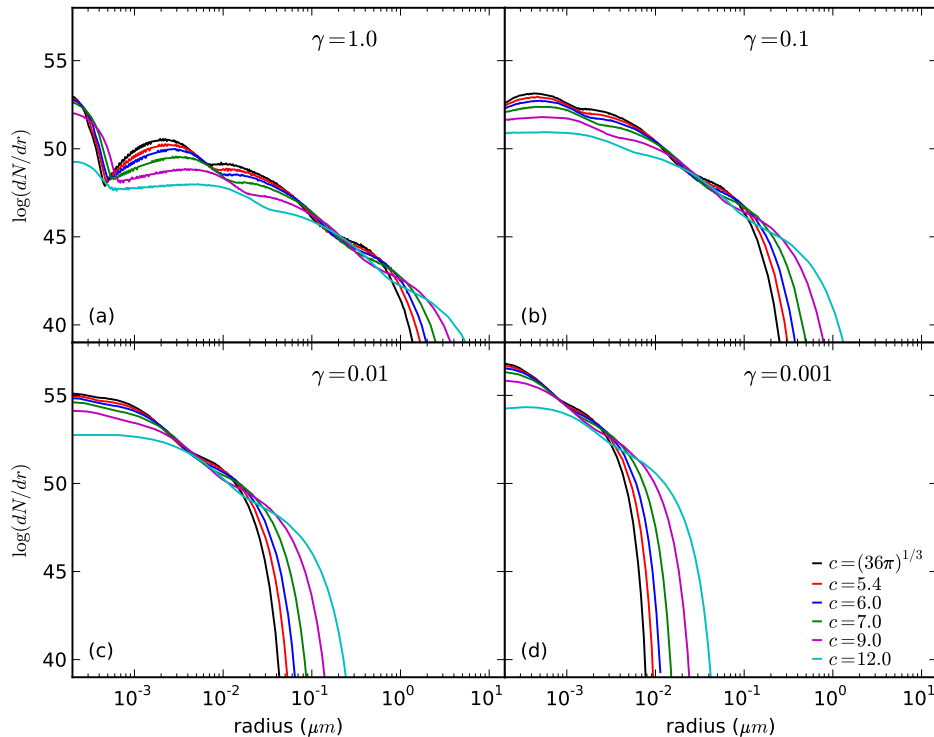


Figure 13. Size distribution of carbon grains for six shape factors and four sticking coefficients.

The dust that condenses, however, is not the dust that is ejected into the ISM. Dust produced in a CCSN has to travel through the reverse shock before being released into the ISM. The reverse shock can destroy most of the dust, in particular the smaller dust grains (Draine & Salpeter 1979; Nozawa et al. 2007; Nath, Laskar, & Shull 2008; Silvia, Smith, & Shull 2010). If astrophysical dust formation is indeed characterized by small values of the sticking coefficient, it is likely that the amount of dust formed is reduced significantly by the reverse shock. Conversely, increased shape factors allow for the formation of larger grains which would survive shock processing. The microphysical properties of dust grains can therefore affect the mass of dust that is injected in the interstellar medium, even though they affect only marginally the dust that is condensed during the early stages of the explosion.

Grain nucleation with non-spherical shapes may be more complicated than we considered here. We have assumed that the shape factors of the grains do not change as the grains grow. Since we assume here that grains grow by the addition of monomers, the shape of small clusters can change as monomers attach, in turn altering the shape factor. Another route to take could be to nucleate grains at an arbitrary shape factor and then allow the grains to grow into spheres. For example, one may turn grains into spheres when the number of monomers is larger than a given value. In this case, increased shape factors may not lead to such large grains as we show in our size distributions (Figure 13).

This work is purely a parametric study that aims to

show that the microphysical properties of the grains are important, but not to point to any specific values of γ and c to be used in nucleation calculations. Therefore, we have chosen to neglect important factors that need be considered in a complete SN dust nucleation model. These include the choice of progenitor model, the presence of other dust species (see Nozawa et al. (2003)) as well as charged molecules that may interfere with carbonaceous dust condensation, and the destruction of CO molecules, due to photodissociation or collisions with fast electrons and charged particles (Petuchowski et al. 1989; Lepp, Dalgarno, & McCray 1990; Liu, Dalgarno, & Lepp 1992; Clayton, Deneault, & Meyer 2001), that can inject additional carbon atoms into the available monomer concentration (see Todini & Ferrara (2001); Bianchi & Schneider (2007)).

A zero-metallicity 20 M_{\odot} CCSN progenitor model was chosen because SNe at high redshift are expected to have zero metallicity. In general, the relative abundances of major elements in the He core are not significantly different among the SN models with different metallicities. Thus, the species of dust formed do not depend on the metallicity of the SN progenitor star (Nozawa et al. 2010). Additionally, the gas density and temperature in the He core are almost independent of the progenitor mass and metallicity as long as the kinetic energy of the explosion is the same (Nozawa et al. 2003). Therefore, SN models with non-zero metallicities, or with different progenitor masses, are expected to show similar effects on carbon grains formation as we see here. This means that the mass of carbon dust formed in the SN ejecta

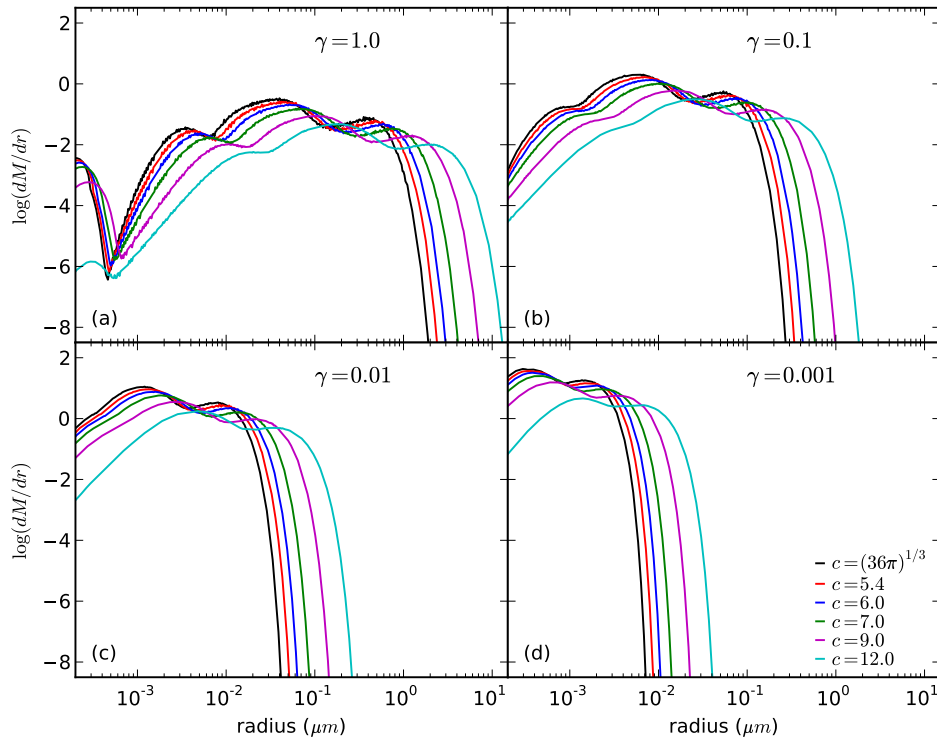


Figure 14. Mass distribution of carbon grain for six shape factors and four sticking coefficients.

is rather insensitive to changes in the sticking coefficient and shape factor and is purely determined by the mass of carbon atoms available for dust formation in the He layer. However, to confirm such expectations, additional progenitor models would need to be investigated.

Perhaps more important than the choice in progenitor model is the dissociation process of CO molecules. In this paper we assumed the formation of CO molecules to be complete and considered only the condensation process of C grains in the He layer where $C/O > 1$. In the expanding ejecta, CO molecules could be destroyed through interactions with fast electrons from radioactively decaying ^{56}Co and charged particles such as He^+ and Ne^+ (Petuchowski et al. 1989; Lepp, Dalgarno, & McCray 1990; Liu, Dalgarno, & Lepp 1992; Clayton, Liu, & Dalgarno 1999; Kwong, Chen, & Fang 2000; Clayton, Deneault, & Meyer 2001; Deneault, Clayton, & Meyer 2006), allowing for more free carbon (and oxygen) atoms to be available for grain formation than we consider here. However, the number abundance of silicon atoms is too small for most of the enclosed mass regions ($M = 4.93\text{--}6.21 M_{\odot}$) in this work (see Figure 3), so that the formation of SiC and silicate grains cannot be expected. Therefore, the dissociation of CO molecules due to interactions with He^+ only results in a slight enhancement of the final mass of carbon grains and never changes our conclusion on the dependence of formation process of C grains on the microphysical properties.

On the other hand, Clayton, Liu, & Dalgarno (1999) and Deneault, Clayton, & Meyer (2006) show that CO dissociation enables carbon dust grains to form even in O-rich layer where $C/O < 1$. Given that the abundance of silicon atoms in the O-rich layer is higher than in the He layer, the formation of SiC grains could be expected there. However, as discussed in Nozawa et al. (2003), even if free carbon and silicon atoms coexist abundantly, the nucleation theory does not predict the formation of SiC grains. The formation process of large SiC grains as appeared in presolar grains, as well as formation efficiency of molecules is to be pursued in more sophisticated studies of dust formation. Furthermore, in the O-rich layer, the formation of silicate grains is also feasible. Bianchi & Schneider (2007) show that the formation of silicate grains is more sensitive to changes in sticking coefficient than carbon grains, and the mass of silicate grains formed can be reduced for even $\gamma = 0.1$. The inclusion of silicate grains could affect the resulting extinction curves.

We have adopted the thermodynamic approach for this study because it involves the simplest nucleation equations, however, use of the kinetic theory of nucleation should be considered in the future. The kinetic theory still needs to take the sticking coefficient into account, but makes consideration of an evolving shape factor unnecessary, because the shape of the grain from a complex solid (for a few molecules) to a sphere (for ~ 100 molecules) is intrinsically taken into account.

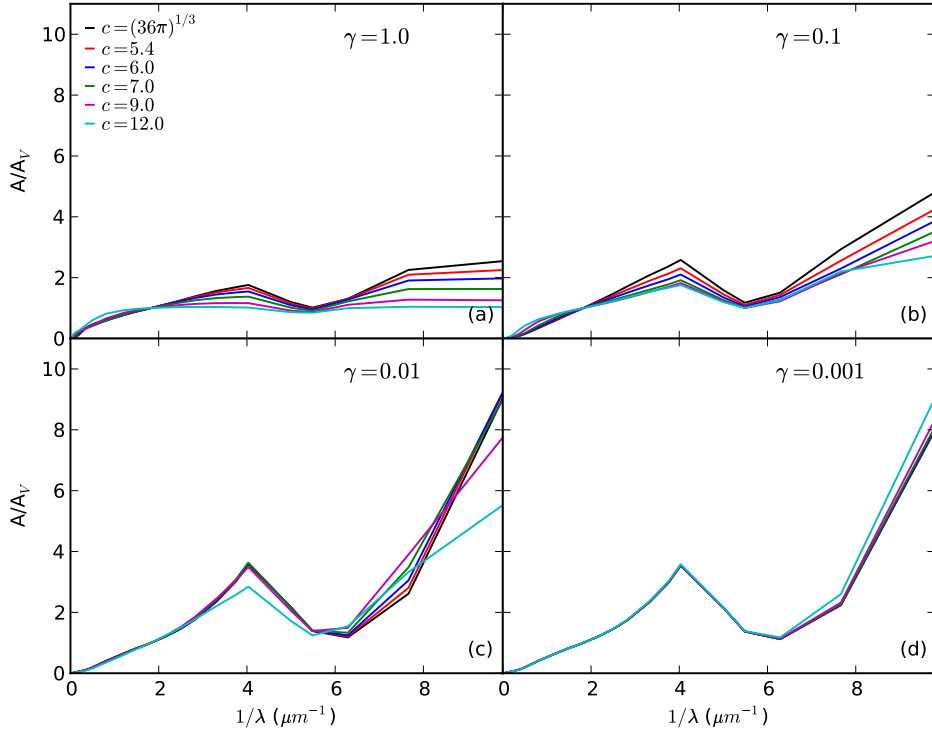


Figure 16. Extinction curves for each sticking coefficient and shape factor.

ACKNOWLEDGEMENTS

We would like to thank the reviewer for their insightful comments and suggestions for the improvement of this work. We would also like to thank Raffaella Schneider and Andrea Ferrara for their comments. Thanks go to the Institute for the Physics and Mathematics of the Universe (IPMU), University of Tokyo, Kashiwa, Japan, for their generous hospitality, and to the NSF East Asia and Pacific Summer Institute (EAPSI) Japan 2010 program (award #1015575) and the Japanese Society for Promotion of Science for their generous support. This work has also been supported in part by World Premier International Research Center Initiative, MEXT, Japan.

REFERENCES

- Barlow M. J., et al., 2010, *A&A*, 518, L138
 Becker R., & Döring W., 1935, *Ann. Phys.*, 24, 719
 Bianchi S., Schneider R., 2007, *MNRAS*, 378, 973
 Bromm V., Coppi P. S., Larson R. B., 2002, *ApJ*, 564, 23
 Cherchneff I., 2010, *ASPC*, 425, 237
 Cherchneff I., Dwek E., 2009, *ApJ*, 703, 642
 Cherchneff I., Dwek E., 2010, *ApJ*, 713, 1
 Clayton D. D., Deneault E. A.-N., Meyer B. S., 2001, *ApJ*, 562, 480
 Clayton D. D., Liu W., Dalgarno A., 1999, *Sci*, 283, 1290
 Deneault E. A.-N., Clayton D. D., Meyer B. S., 2006, *ApJ*, 638, 234
 Donn B., Nuth J. A., 1985, *ApJ*, 288, 187
 Douvion T., Lagage P. O., Cesarsky C. J., 1999, *A&A*, 352, L111
 Draine B. T., Salpeter E. E., 1979, *ApJ*, 231, 438
 Dwek E., Galliano F., Jones A. P., 2007, *ApJ*, 662, 927
 Elmhamdi A., et al., 2003, *MNRAS*, 338, 939
 Elvis M., Marengo M., Karovska M., 2002, *ApJ*, 567, L107
 Feder J., Russell K. C., Lothe J., Pound G. M., 1966, *Adv. Phys.*, 15, 111
 Hoyle F., Wickramasinghe N. C., 1970, *Nature*, 226, 62
 Kashchiev D., 2000, *Nucleation: Basic Theory With Applications*, Butterworth-Heinemann, Oxford
 Keith A. C., Lazzati D., 2011, *MNRAS*, 410, 685
 Kotak R., et al., 2009, *ApJ*, 704, 306
 Kozasa T., Hasegawa H., 1987, *PThPh*, 77, 1402
 Kozasa T., Hasegawa H., Nomoto K., 1989, *ApJ*, 344, 325
 Kozasa T., Hasegawa H., Nomoto K., 1991, *A&A*, 249, 474
 Kozasa T., Nozawa T., Tominaga N., Umeda H., Maeda K., Nomoto K., 2009, *ASPC*, 414, 43
 Kwong V. H. S., Chen D., Fang Z., 2000, *ApJ*, 536, 954
 Lazzati D., 2008, *MNRAS*, 384, 165
 Lepp S., Dalgarno A., McCray R., 1990, *ApJ*, 358, 262
 Li A., Greenberg J. M., 2003, *ssac.proc*, 37
 Liu W., Dalgarno A., Lepp S., 1992, *ApJ*, 396, 679
 Lucy L. B., Danziger I. J., Gouffes C., Bouchet P., 1989, *LNP*, 350, 164
 Maiolino R., Schneider R., Oliva E., Bianchi S., Ferrara A., Mannucci F., Pedani M., Roca Sogorb M., 2004, *Nature*, 431, 533

- Mathis J. S., Rumpl W., Nordsieck K. H., 1977, *ApJ*, 217, 425
- Meikle W. P. S., et al., 2007, *ApJ*, 665, 608
- Morgan H. L., Edmunds M. G., 2003, *MNRAS*, 343, 427
- Nomoto K., Tominaga N., Umeda H., Kobayashi C., Maeda K., 2006, *NuPhA*, 777, 424
- Nozawa T., Kozasa T., Umeda H., Maeda K., Nomoto K., 2003, *ApJ*, 598, 785
- Nozawa T., Kozasa T., Habe A., Dwek E., Umeda H., Tominaga N., Maeda K., Nomoto K., 2007, *ApJ*, 666, 955
- Nozawa T., et al., 2008, *ApJ*, 684, 1343
- Nozawa T., Kozasa T., Tominaga N., Maeda K., Umeda H., Nomoto K., Krause O., 2010, *ApJ*, 713, 356
- Nath B. B., Laskar T., Shull J. M., 2008, *ApJ*, 682, 1055
- Petuchowski S. J., Dwek E., Allen J. E., Jr., Nuth J. A., III, 1989, *ApJ*, 342, 406
- Rho J., et al., 2008, *ApJ*, 673, 271
- Sibthorpe B., et al., 2010, *ApJ*, 719, 1553
- Silvia D. W., Smith B. D., Shull J. M., 2010, *ApJ*, 715, 1575
- Stratta G., Maiolino R., Fiore F., D’Elia V., 2007, *ApJ*, 661, L9
- Sugerman B. E. K., et al., 2006, *Sci*, 313, 196
- Temim T., Slane P., Reynolds S. P., Raymond J. C., Borkowski K. J., 2010, *ApJ*, 710, 309
- Todini P., Ferrara A., 2001, *MNRAS*, 325, 726
- Umeda H., Nomoto K., 2002, *ApJ*, 565, 385
- Valiante R., Schneider R., Bianchi S., Andersen A. C., 2009, *MNRAS*, 397, 1661
- Wooden D. H., Rank D. M., Bregman J. D., Witteborn F. C., Tielens A. G. G. M., Cohen M., Pinto P. A., Axelrod T. S., 1993, *ApJS*, 88, 477
- Wooden D. H., 1997, *AIPC*, 402, 317
- Zhukovska S., Gail H.-P., Tieloff M., 2008, *A&A*, 479, 453